Available online at www.sciencedirect.com
ScienceDirect
Optics Communications 281 (2008) 3327–3335
OPTICS COMMUNICATIONS
www.elsevier.com/locate/optcom

Generation of powerful filaments at a long distance using adaptive optics

J.-F. Daigle [a,*], Yousef Kamali [a], Jens Bernhardt [a], Weiwei Liu [b], Claude Marceau [a], A. Azarm [a], S.L. Chin [a]

[a] Centre d'Optique, Photonique et Laser (COPL) et le Département de Physique, de Génie Physique et d'Optique, Université Laval, Québec, Canada G1K 7P4

[b] Institute of Modern Optics, Nankai University, Key Laboratory of Opto-electronic Information Science and Technology, Education Ministry of China, Tianjin 300071, China

Received 31 December 2007; received in revised form 22 February 2008; accepted 22 February 2008

Abstract

Because of its extraordinary properties (intensity clamping, white light source, km long plasma channels), filamentation represents an ideal candidate for remote sensing. However, the promising generation of filaments at long distances for such purposes remains an issue.

We propose a specially designed focusing telescope to properly deliver the laser pulses at long distance and generate powerful filaments. The telescope includes a deformable mirror (DM) that corrects the wavefront's aberrations working in a closed loop system with a wavefront sensor (WFS). Using this setup we are able to generate extraordinarily strong nitrogen signals at a distance as far as 90 m using 40 mJ laser pulses. Compared to the chirped based filament control technique, we believe that an appropriate control of the reservoir like what we have achieved will contribute to reduce the energy of the required laser pulses and at the same time, the cost of the required laser system.

1. Introduction

When propagating in the atmosphere, the non-linear behavior of intense ultrashort laser pulses leads to the formation of long plasma channels with unique properties. Their discovery [1] awoke the interest of many researchers in the field of non-linear optics to pursue atmospheric studies using these structures nowadays called filaments [2–5]. They represent a potential breakthrough towards the development of atmospheric tools in the fields of LIDAR remote sensing [6–8] and electric discharge triggering/guiding [9,10], for example.

In the atmosphere, the filaments appear as a dynamic equilibrium between Kerr self-focusing and self-defocusing by the self-generated low-density plasma produced by multiphoton/tunnel ionization of the air molecules [2]. Indeed, for a non-uniform intensity distribution laser pulse (Gaussian, for example) with peak power higher than the critical power for self-focusing, the Kerr effect will act as a non-linear lens that will focus the light pulse until its intensity is sufficiently high to ionize the medium in which it propagates. The critical power is defined as

$$P_{\mathrm{crit}} = 3.77\lambda^2/8\pi n_0 n_2$$

where λ is wavelength, n_0 is the medium's linear refractive index and n_2, the second order non-linear refractive index. Once the plasma is sufficiently dense to counteract the Kerr lens effect, the laser pulse will start to defocus. The defocusing nature of the plasma limits and stabilizes the light intensity in each of the filaments. In air, the clamped intensity is approximately 5×10^{13} W/cm^2 [11,12].

Filamentation intensity clamping represents an incredible advantage for atmospheric studies. In linear regimes, diffraction limits the intensity that can be delivered around

* Corresponding author.
E-mail address: jfdaigle2@yahoo.ca (J.-F. Daigle).

0030-4018/$ - see front matter © 2008 Elsevier B.V. All rights reserved.
doi:10.1016/j.optcom.2008.02.036

the focal point of any focusing device. Assuming a Gaussian beam, the beam diameter will linearly increase with the focal distance following the relation:

$$\Delta\phi = 4f\lambda/\pi D \tag{1}$$

where $\Delta\varphi$ is the focal diameter, f is the effective focal length of the device, λ is the wavelength of the incident light and D is the input beam diameter. Thus, the intensity around the focal plane of a 10 J/10 ns/532 nm laser pulse focused at 500 m and 1 km would be respectively limited at 5×10^{10} W/cm^2 and 1.25×10^{10} W/cm^2. This intensity will continue to go down with an increasing focal length. On the other hand, the filament's clamped intensity (5×10^{13} W/cm^2) provides non diffraction limited ionization zone of constant and uniform intensity throughout its entire filament zone, independent of the focusing distance and the pulse duration/energy. Nevertheless, the formation of filaments suitable for atmospheric studies at long distance remains an issue; a system to adequately control the onset of filaments at atmospheric-scale distances has to be designed.

A method to delay the onset of filaments consists of launching negatively chirp laser pulses so that the normal group velocity dispersion (GVD) of the medium (atmosphere) is precompensated to suit the desired collapse distance [13,14]. Another method proposed by Jin et al. [15] consists of using an adaptive optic to modify the initial divergence of the laser pulses. They demonstrated that the collapse position increased with the beam divergence. They also suggested that the number of filaments generated could be changed by modifying the initial peak power of the pulses. Another method proposed consisted of using astigmatism to control the number of filaments and their stability and a long distance [16].

However, high power laser pulses emitted from the popularly used Ti–sapphire amplifiers have relatively large diameters and relatively low quality spatial profiles. The hot zones generated will each tend to self-focus into a filament. This is the phenomenon of multiple filamentation [17]. Multi-filaments arising from such relatively large diameter pulses are widely spaced and compete for the energy inside the limited reservoir of the pulse resulting in a low number of random filaments [18].

A technique to avoid or minimize this competition is to reduce the beam diameter such that when they self focus, the various hot zones will 'cooperate' and the electric field distribution of and around each filament will undergo constructive interference with the others. This interference occurs because the filaments are now very close to one another. In addition, their formation is enhanced with an optimal use of the closely available energy reservoir. This idea was indeed proven valid by Luo et al. who have increased the N_2 fluorescence signal by more than three orders of magnitude with laser pulses of initial diameter three times smaller [18]. However, in this case, filamentation started rather early and the self-focusing position could not be changed naturally by increasing the negative chirp or the beam divergence. This is because when the laser beam diameter is decreased, the hot zones' diameters are also reduced and forced together around the beam center. According to the Marburger formula [19],

$$z_f = \frac{0.367ka^2}{\left\{\left[\left(\frac{P}{P_{crit}}\right)^{1/2} - 0.852\right]^2 - 0.0219\right\}^{1/2}} \tag{2}$$

for the same peak power (P), a smaller diameter ($d = 2a$) hot zone would lead to a shorter self-focal distance (z_f). Therefore, a smaller beam produces powerful filaments but causes early filamentation.

Liu et al. [20] proposed a method to properly control the filaments at long distances that combines beam expansion and geometrical focusing. The device consists of a 5 cm diameter convex mirror, whose focal length is −50 cm, and a focusing lens with focal length of 100 cm (diameter of 8 cm). The focusing lens was installed on a motorized stage, allowing a variable effective focal length. The purpose of the device is to generate energetic filaments at a far distance. In order to counter the unwanted effects of multiple filamentation competition for the energy in the reservoir, the hot spots are stretched by increasing the beam diameter with the convex mirror. This process delays the onset of filaments. In fact, from (2), a larger beam diameter leads to an increased self-focusing distance. The converging lens is adjusted so that the geometrical focus is much shorter than the non-linear focus. This means that all the energy contained inside the reservoir is merged around the geometrical focusing area where a sudden generation of strong constructively interfering filaments occurs. However, as the focusing distance increases, the validity of the approximation is not accurate anymore. In fact, because of the limited lens size, the difference between the self focal and geometrical distance becomes larger for longer focal distances and leads to multiple filament competition.

In an attempt to increase the filamentation onset distance, a new telescope that could further increase the beam diameter was designed. Since it is difficult to build a large diameter lens sufficiently thin to prevent nonlinearities in the bulk material, it consists of two slightly off-axis reflective optics: a convex dielectric mirror of −25 cm focal length followed by a 1 m focal length aluminium coated concave mirror. The concave mirror can handle beam diameters as large as 15 cm. In theory, such a large beam size places the non-linear focus at approximately 5 km Eq. (2) and allows kilometer range applications. Unfortunately, because of the tilted mirrors, the telescope proved itself as being inappropriate for this purpose. Fig. 1 shows the images that were taken with a CCD camera looking at the 800 nm/50 mJ negatively-chirped-1 ps pulse scattering from a white sheet of paper located at regularly spaced positions along the propagation axis. The beam pattern is highly astigmatic and in these conditions, no strong filaments were produced. In this work, we would like to report

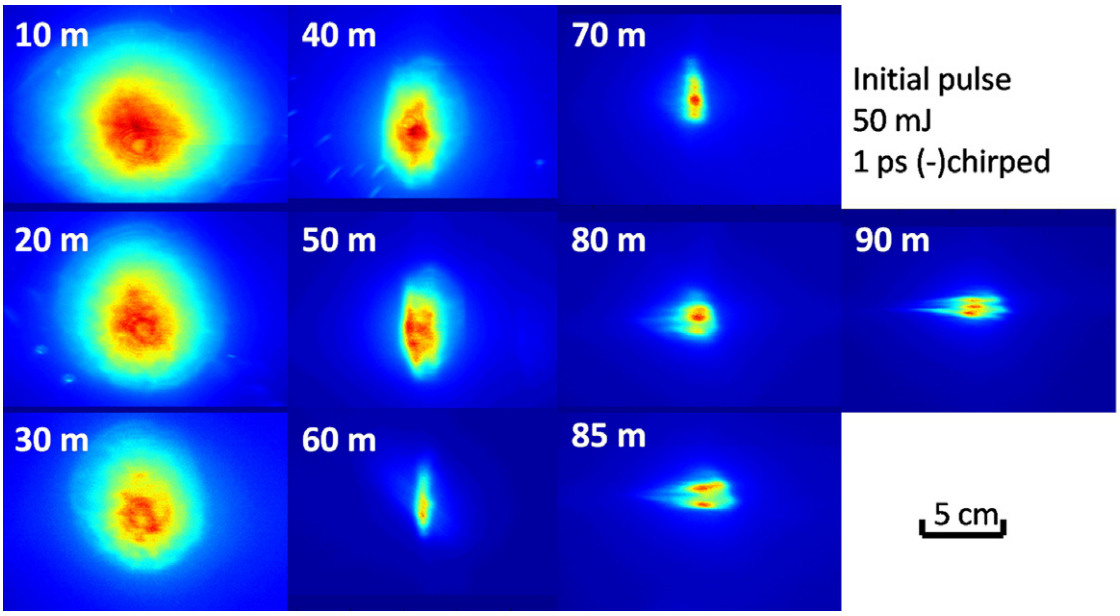

Fig. 1. Beam patterns measured with a CCD camera looking at the uncorrected 800 nm/50 mJ negatively-chirped-1 ps pulse scattering from a white sheet of paper located at regularly spaced positions along the propagation axis.

on how an adaptive optic was used to solve the astigmatism problem and generate powerful filaments for atmospheric studies.

2. Propagation control setup

In this experiment, the filaments were produced with the same laser pulses at different energies. These pulses were focused through a 30 m long corridor with the variable focal length sending telescope presented in Fig. 2. The telescope consists of a 5 cm diameter convex deformable mirror DM (Visionica Ltd.) [21] of −25 cm focal length mounted on a translation stage followed by a 20 cm diameter aluminum coated concave mirror. It is working in a closed loop system with a Shack–Hartmann wavefront sensor (WFS) located after the delivering telescope. The sensor observes the wavefront transmitted through a leaking 10 cm diameter wedge with dielectric coating on one side that reflects 99% of the beam's energy towards the target. Based on the measured/calculated wavefront, a genetic algorithm automatically drives the various deformable mirror's actuator groups to obtain a nearly flat wavefront.

The Shack–Hartmann detector works as follows. The wavefront leaking through the wedge is imaged on a 2D array of 1000 lenslet. Each lenslet focuses the local wavefront on a CCD camera located at the lenslet's focal plane. Fig. 3a shows the CCD image of an arbitrary wavefront. Any local phase shift of the wavefront transmitted through a lenslet will be deviated, on the CCD plane, with respect to the lenslet axis (Fig. 3b). Based on each deviation, the local phase shifts can be calculated to reconstitute the entire wavefront's phase. Then, the genetic algorithm of the

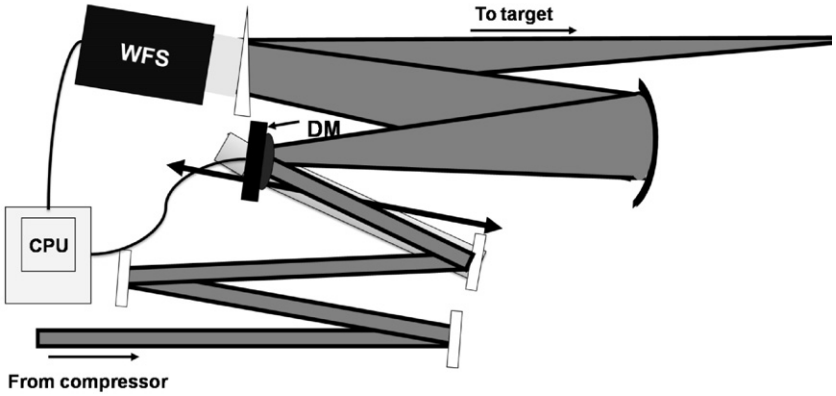

Fig. 2. Schematic of our specially designed focusing telescope. The setup includes a deformable mirror and a wavefront sensor working in a closed loop system to correct the induced aberrations.

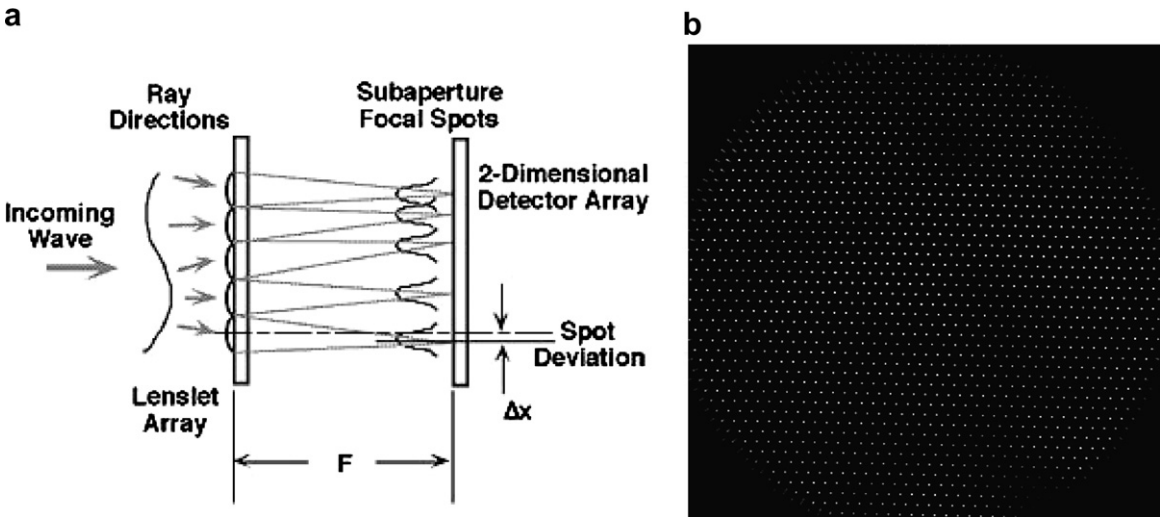

Fig. 3. (a) Shack–Hartmann wavefront sensor schematic. (b) A CCD image from an arbitrary wavefront measured with the wavefront sensor.

closed loop system drives each actuator groups of the mirror to obtain a nearly flat wavefront at the exit of the sending telescope.

The deformable mirror consists of 16 thin plates of piezoceramic material coupled to a glass substrate. The expansion/contraction of the piezoceramic plate is controlled by the polarization and magnitude of the voltage applied to an individual actuator. The voltage is applied throughout a network of electrodes deposited on the inner side of the substrate. On the outer side, a dielectric coating has been deposited to optimize the reflectivity around 800 nm.

A genetic algorithm allows cooperative work between the deformable mirror and the wavefront sensor. It is designed to automatically correct to a flat wavefront. Instead of testing random piezoceramic plates, the algorithm controls different groups of actuators that correct for specific aberrations. Fig. 4 presents the wavefront's deformation produced by two of the eleven preprogrammed actuator groups. The images correspond to the interferograms between the wavefronts measured without and with mirror correction. Fig. 4a and b shows the defocusing and astigmatic actuator groups respectively. As expected, the defocusing group induces a phase shift along the radial direction and the astigmatic group induces a phase shift between orthogonal directions. The genetic algorithm optimizes the voltages applied to each of the groups to obtain the optimal wavefront.

3. Experiments and results

The beam was folded twice at each end of the corridor with dielectric mirrors reflecting around 800 nm at 0° incidence angle. The effect of the deformable mirror is thus tested for laser pulses propagating up to 90 m. The beam

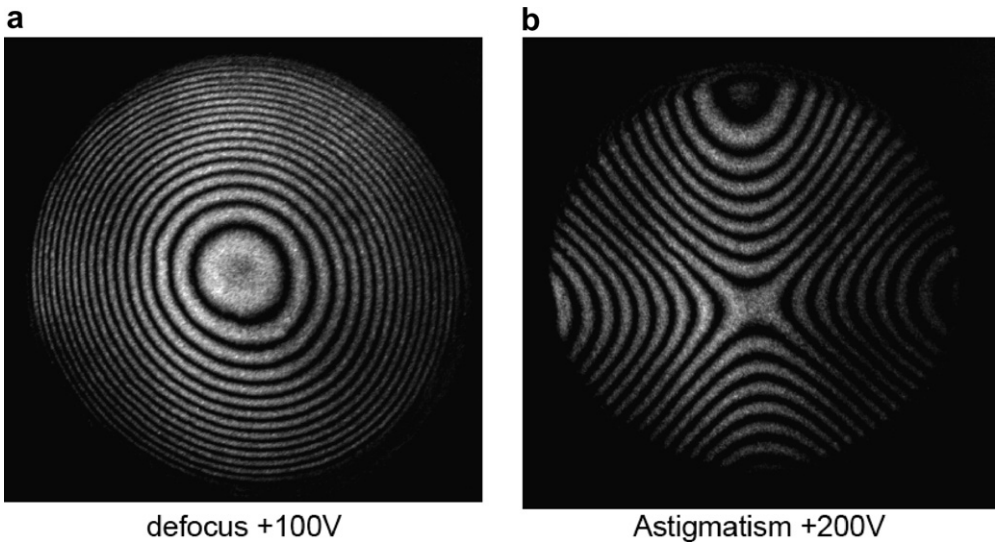

Fig. 4. (a) Interferogram of the defocusing group. (b) Interferogram of the astigmatic group.

profile is characterized as a function of the propagation distance with a CCD camera looking at the laser scattering from a white sheet of paper. The beam profiles are shown in Fig. 5. A comparison with the uncorrected beam patterns (Fig. 1) shows that the laser's astigmatic behavior was significantly reduced. But more importantly, the focal area at 85 m is more than 16 times smaller for the corrected pulses. This energy reservoir confinement around the focal area will greatly enhance the probability of filaments' formation at long distances.

The filaments were characterized using the molecular fluorescence emitted from N_2 present in air which was detected in a LIDAR [22] configuration. It consists of a 28 cm diameter mirror of 1.5 m focal length and a gated photomultiplier tube (PMT) positioned near the mirror's focal length. The detected signal was filtered using a 4 mm thick UG11 filter [24] and a 800 nm dielectric mirror positioned in front of the gated PMT. The geometric focal length of the telescope is approximately 78 m. The LIDAR was positioned near the sending telescope and the PMT gating was adjusted so that only the segment with filamentation is observed (60–90 m). Therefore, the laser beam propagated over 90 m, but the LIDAR looked from a distance ranging from 5 m to 30 m. And the LIDAR equation has been used to calibrate the obtained signals up to 90 m. This extrapolation would be much more accurate than previous extrapolation [8] since we do not make any assumption of the filament length.

Characteristic signal traces retrieved from the oscilloscope are shown in Fig. 6. For this experiment, the filaments were generated from 1 ps negatively chirped laser pulses of energies ranging from 30 to 50 mJ. The horizontal axis corresponds to the time elapsed from the trigger, but it has been calibrated to represent the laser propagation distance. Each trace was accumulated for 2500 laser pulses.

In this figure, the two first peaks on the left is noise induced by the PMT's gating signal and the peak at the right hand side is the white light scattering from the beam dump located at the end of the corridor. In between, the fluorescence signal detected provides important information concerning the position and length of the filament structure. In the present case, the filaments were formed after 72 m propagation and ended around 77 m.

We then decided to repeat this set of experiment using longer pulse durations. The results are presented in Fig. 7. Each data point corresponds to the integrated N_2 fluorescence signal measured by the gated PMT. From these plots, we observe that as the pulse duration is shortened, the detected fluorescence signal increases significantly. But more importantly, a 40 mJ/1 ps negatively chirped pulse can produce the same signal as a 50 mJ/5 ps negatively chirped pulse. This signal enhancement is due to the increased pulse power which would normally lead to the formation of more individual filaments. However, it has been reported [17] that short pulses multiple filamentation often generate weak and random fluorescence signals. Another scenario is that the wavefront of the pulse is sufficiently smooth to produce, near the geometrical focusing area, a single and powerful structure embedding all the produced multi-filaments. In this case, constructive

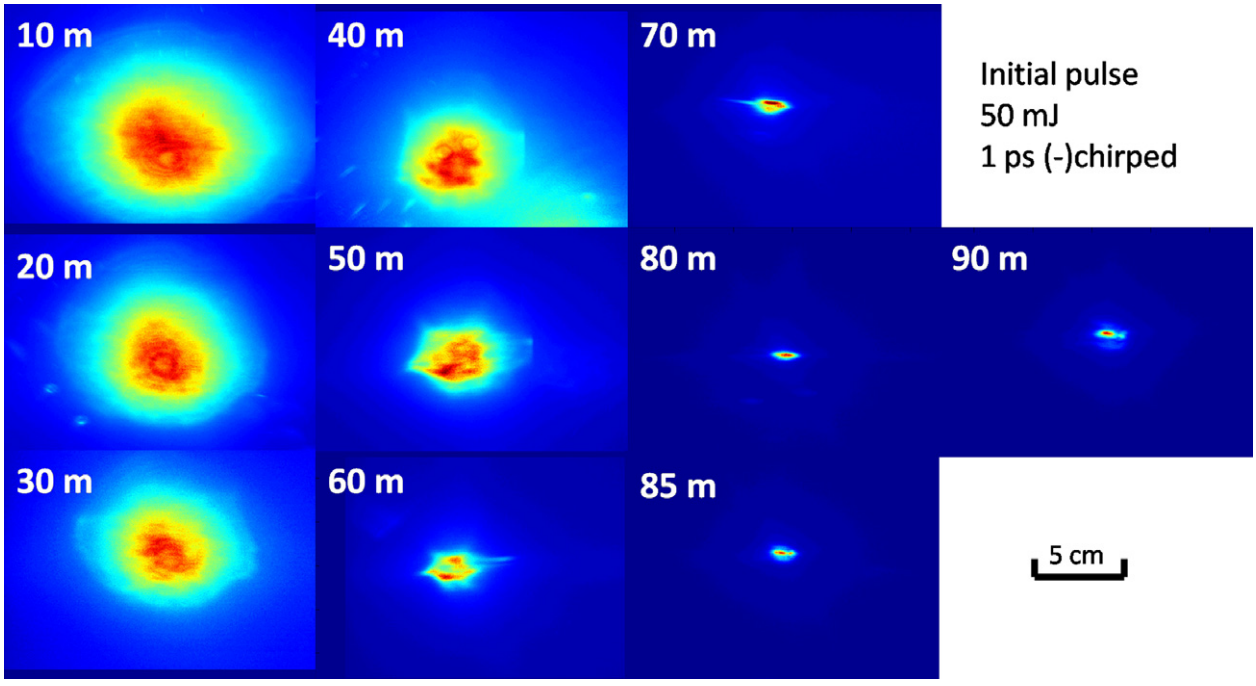

Fig. 5. Beam patterns measured with a CCD camera looking at the corrected 800 nm/50 mJ negatively-chirped-1 ps pulse scattering from a white sheet of paper located at regularly spaced positions along the propagation axis.

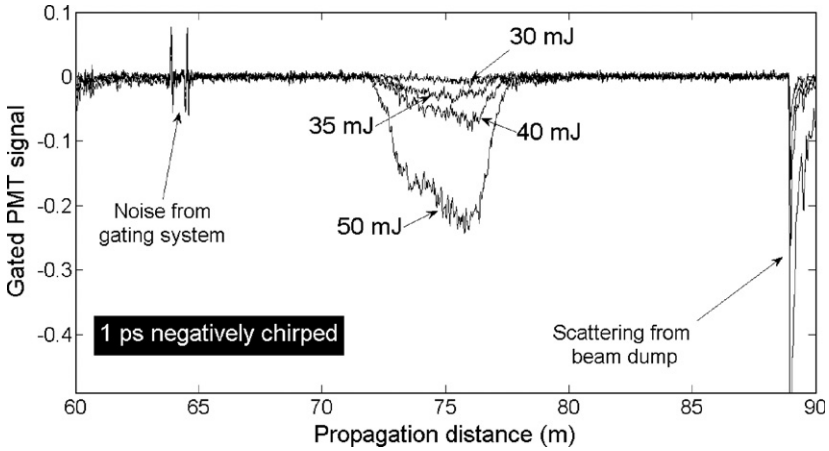

Fig. 6. Gated PMT trace measured in a LIDAR configuration for various pulse energies (1 ps negatively chirped).

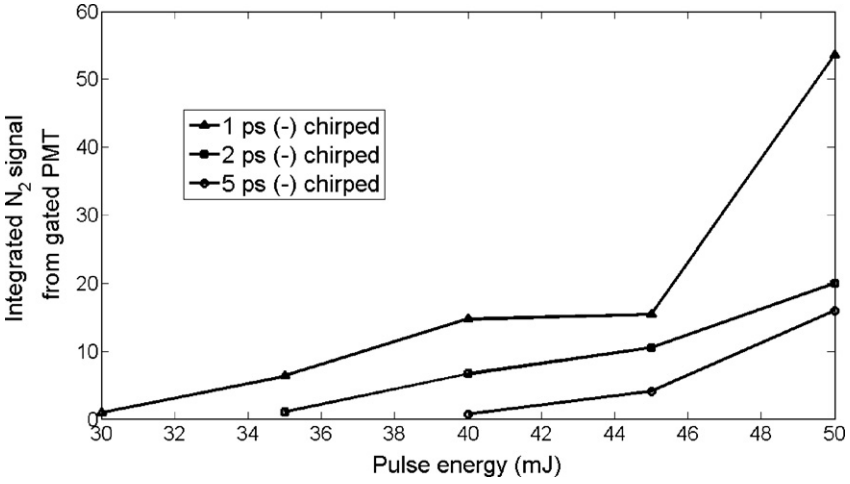

Fig. 7. Integrated N_2 fluorescence signal plotted as a function of the pulse energies and pulse durations.

interference of the many filaments [18] generated would significantly enhance the measured fluorescence signal.

We performed another experiment to observe the laser pulses' transverse beam profiles near the focal zone. This time, the telescope focal length was fixed at 85 m where a thick polished piece of bulk fused silica glass was placed at a grazing angle (15° with respect to laser propagation) inside the filamentation zone formed by focused corrected pulses. The first surface's reflection was sent towards a CCD detector protected by a neutral density filter of 0.009% transmission. Fig. 8 shows three pictures taken when 35, 40 and 45 mJ laser pulses propagated in the corridor. These filaments' patterns suffer from shot-to-shot fluctuations. However, these three images provide important informations concerning long distance filamentation onset. In fact, a comparison between Fig. 8a and b shows that the energy threshold for the collapse into filaments at 85 m is approximately 40 mJ. At this energy, multi-filaments are formed. As the energy is increased, the multi-filaments feeding from the focused energy reservoir undergo constructive interference. Because of intensity clamping, the filaments produced with higher energies have larger diameters [23]. As the pulse's energy increases further, each separate filament grows bigger and eventually merges into its neighbors; i.e. these filaments fuse into a larger structure (Fig. 8c, 45 mJ).

In order to characterize the plasma inside the filament, a photomultiplier tube (PMT) isolated by a UG11 filter [24] and a 800 nm dielectric mirror, positionned at 85 m, measured the N_2 fluorescence from the side of the filament. Fig. 9 shows the PMT signal averaged over 512 laser shots as a function of the pulse energy for the uncorrected and corrected wavefronts. From 5 mJ to 60 mJ, no significant fluorescence was emitted when the deformable mirror was inactive, i.e. no filaments were created. On the other hand, when the mirror correction was applied, strong signals were detected starting at 45 mJ. These results confirm that constructive interference of the filaments sharply increases the plasma generation. In fact, as the pulse energy increases from 40 mJ to 45 mJ, the fluorescence detected increased by a factor of four. Fig. 8b shows the beam pattern for the 40 mJ case. The few multiple hot spots give rise to a

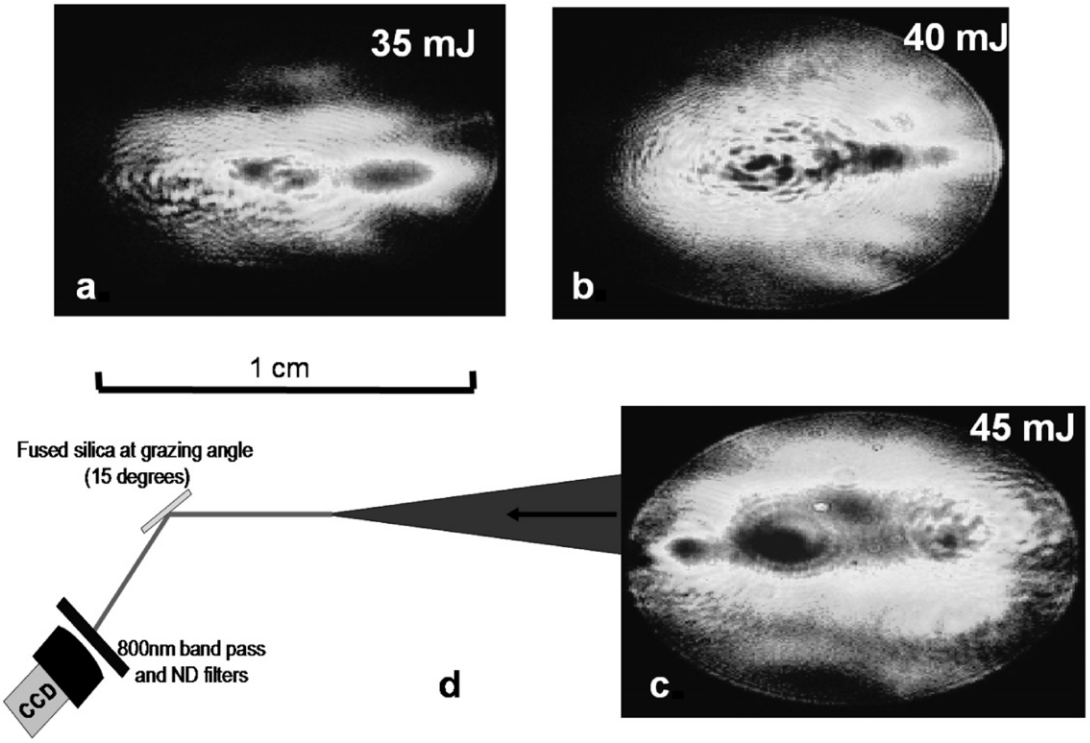

Fig. 8. CCD images retrieved from the reflection of a thick fused silica sample located near the geometrical focus area (d). At 40 mJ (a), no filaments are observed, at 45 mJ (b), well separated multi-filaments are observed and at 50 mJ (c), constructive interference of the multi-filaments is observed.

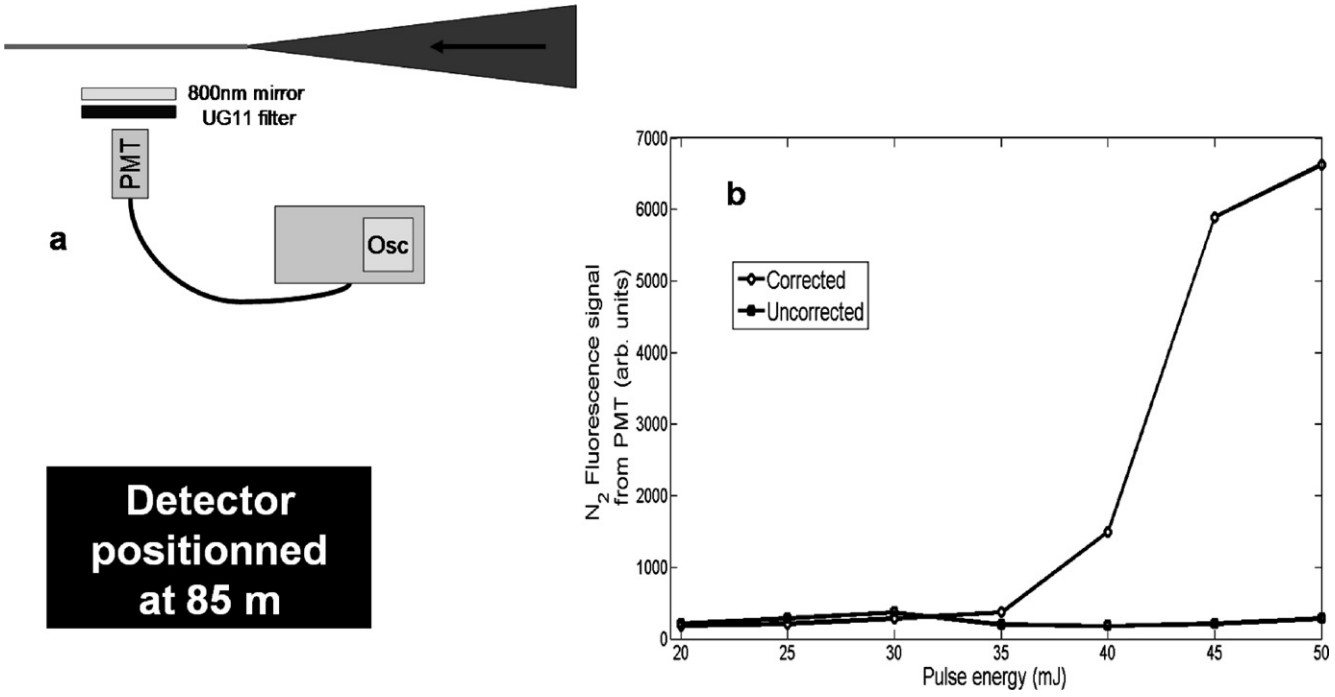

Fig. 9. Integrated N_2 fluorescence signal measured with a PMT in a side imaging configuration (a). The results are plotted for various pulse energies (b).

low fluorescence signal. At 45 mJ, these filaments start to fuse into a tight bundle (Fig. 8c). This effect drastically enhances the emitted fluorescence signal. We believe that this powerful filament bundle is the tool required for efficient atmospheric studies.

4. Discussion

In Ref. [15], only the defocusing group, shown in Fig. 4a, has been used to control the divergence of the laser pulses. They varied the voltage applied to the actuator

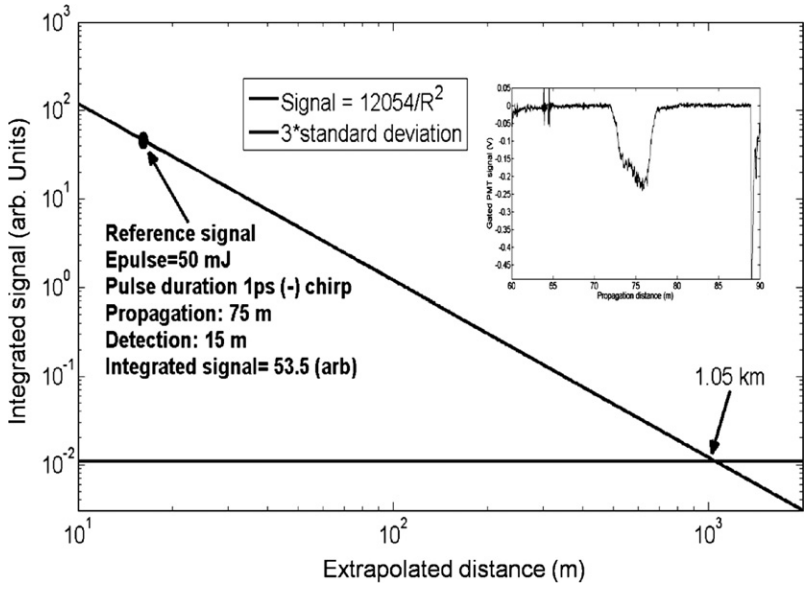

Fig. 10. Extrapolation over distance based on a reference N_2 fluorescence signal measured with a 50 mJ/1 ps negatively chirped pulse.

group that can modify the curvature of the launched wavefront. For this type of control, a wavefront sensor is not required. The purpose of their experiment was to find a convenient method to control the position of the onset of filaments. However, the filaments obtained appear as being inadequate for atmospheric applications. In fact, with 300 GW pulses, the onset of the filaments was delayed to 40 m with a 0.5 mrad diverging pulses. Nonetheless, this collapsing distance is insufficient for atmospheric studies. Moreover, the filaments resulting from large diverging pulses are widely separated; mutiple filamentation competition would be unavoidable and it would generate weak plasmas as was shown in Ref. [17].

In an attempt to improve Liu et al.'s [20] design, we used a deformable mirror working in a closed loop system with a Shack–Hartmann wavefront sensor to correct the aberration induced by a telescope that optimizes filament generation at a long distance. As opposed to Ref. [15], the deformable mirror corrected the astigmatism induced by the focusing device to generate constructively interfering strong filaments at various distances up to 85 m. The limited size (30 m long corridor) of our installations did not allow longer propagation distances. In fact, for focal distances beyond 90 m, the laser beam cannot be folded anymore because of the limited size of our mirrors reflecting the beam at the corridor's ends.

This is why extrapolation based on the LIDAR equation [22] has to be performed to demonstrate that filamentation can be used as a remote sensing tool at atmospheric scale. The gated PMT signal shown in the inset of Fig. 10 was used for the calculation. It was measured with our LIDAR at a distance of approximately 15 m. In this case, the filaments were formed after 75 m propagation with 50 mJ/1 ps negatively chirped pulses. The extrapolation is based under the assumption that it is possible to generate, no matter what the focal distance is, the same signal (filaments) that was obtained at the reference position. As shown in Fig. 10, we expect that the fluorescence signal would be equal to three times the standard deviation if it were produced at 1.05 km. Such a long remote sensing distance would be suitable for most atmospheric and military applications.

As of now, the main limit to the development of atmospheric technologies with intense ultrashort laser pulses is the price of the laser system. In fact, the powerful laser systems required are usually priced at the million dollars (US) level. The development of techniques that optimize filamentation generation at long distances will contribute to reducing the cost of the required laser systems. We demonstrated that with an adequate spatial control of the background reservoir, 35 mJ pulses (Fig. 6) can produce filaments sufficiently powerful to generate an appreciable N_2 fluorescence signal after 75 m of propagation. Moreover, we demonstrated that if the wavefront is sufficiently smooth, increasing the pulse power by reducing its duration can significantly enhance the generated fluorescence. From Fig. 7, we see that a 40 mJ/1 ps negatively chirp pulses can provide the same signal as 50 mJ/5 ps negatively chirp pulses. Therefore, if the pulse energy required to produce the filaments is reduced, the laser systems emitting these pulses would be cheaper, of smaller dimension and more attractive to the industrial sector.

5. Conclusion

We believe that the obtained results are very promising for the development of filamentation technologies for atmospheric applications. We demonstrated that a specially designed sending telescope based on adaptive optics technologies can produce powerful filaments at a long dis-

tance with a relatively low energy level. We showed that these constructively interfering filaments produce strong fluorescence signals and will most probably improve remote sensing measurements at atmospheric scales.

However, there is still some room left for improvements. In fact, from Figs. 5 and 8 the astigmatism is still not totally removed by the deformable mirror. This aberration favors multiple filamentation regime by spreading the energy reservoir away from the propagation axis. For optimum results, the desired beam pattern around the focusing area has to be circular and tightly focused. In this way, the filaments will feed from the intense energy reservoir closely surrounding the tight bundle giving rise to strong fluorescence from the ionized medium.

Acknowledgements

This work was partially supported by NSERC, DRDC-Valcartier, Canada Research Chairs, CIPI, CFI, and FQRNT. We appreciate very much the technical assistance of Mr. Mario Martin. W. Liu acknowledges the support of NSFC (Grant No. 60637020), Chinese National Major Basic Research Development Program (973) (Grant No. 2007CB310403) and NCET.

References

[1] A. Braun, G. Korn, X. Liu, D. Du, J. Squier, G. Mourou, Opt. Lett. 20 (1995) 73.
[2] S.L. Chin, S.A. Hosseini, W. Liu, Q. Luo, F. Théberge, N. Akozbek, A. Becker, V.P. Kandidov, O.G. Kosareva, H. Schroeder, Can. J. Phys. 83 (2005) 863.
[3] L. Wöste, C. Wedekind, H. Wille, P. Rairoux, B. Stein, S. Nikolov, Ch. Werner, S. Niedermeier, H. Schillinger, R. Sauerbrey, Laser Optoelektron. 29 (1997) 51.
[4] M. Mlejnek, E.M. Wright, J.V. Moloney, Opt. Lett. 23 (1998) 382.
[5] A. Couairon, A. Mysyrowicz, Phys. Rep. 441 (2007) 47.
[6] J.-F. Daigle, P. Mathieu, G. Roy, J.-R. Simard, S.L. Chin, Opt. Commun. 278 (2007) 147.
[7] G. Méjean, J. Kasparian, E. Salmon, J. Yu, J.-P. Wolf, R. Bourayou, R. Sauerbrey, M. Rodriguez, L. Wöste, H. Lehmann, B. Stecklum, U. Laux, J. Eislöffel, A. Scholz, A.P. Hatzes, Appl. Phys. B 77 (2003) 357.
[8] Q. Luo, H.L. Xu, S.A. Hosseini, J.-F. Daigle, F. Theberge, M. Sharifi, S.L. Chin, Appl. Phys. B 82 (2006) 105.
[9] S. Tzortzakis, B. Prade, M. Franco, A. Mysyrowicz, S. Hüller, P. Mora, Phys. Rev. E 64 (2001) 057401.
[10] N. Goto, M. Miki, T. Fujii, T. Nayuki, T. Sekika, T. Shindo, K. Nemoto, Trans. Inst. Electr. Eng. Jpn. A 125 (12) (2005) 1059.
[11] Kasparian, R. Sauerbrey, S.L. Chin, Appl. Phys. B: Lasers Opt. 71 (2000) 877.
[12] A. Becker, N. Akozbek, K. Vijayalakshmi, E. Oral, C.M. Bowden, S.L. Chin, Appl. Phys. B 73 (2001) 287.
[13] L. Wöste, C. Wedekind, H. Wille, P. Rairoux, B. Stein, S. Nikolov, C. Werner, S. Niedermeier, F. Ronnenberger, H. Schillinger, R. Sauerbrey, Laser Optoelektron. 29 (1997) 51.
[14] P. Sprangle, J.R. Penano, B. Hafizi, Phys. Rev. E 66 (2002) 046418.
[15] Z. Jin, J. Zhang, M.H. Xu, X. Lu, Y.T. Li, Z.H. Wang, Z.Y. Wei, X.H. Yuan, W. Yu, Opt. Express 13 (2005) 10424.
[16] Gadi Fibich, Shmuel Eisenmann, Boaz Ilan, Arie Zigler, Opt. Lett. 29 (15) (2004) 1772.
[17] S.A. Hosseini, Q. Luo, B. Ferland, W. Liu, S.L. Chin, O.G. Kosareva, N.A. Panov, N. Aközbek, V.P. Kandidov, Phys. Rev. A 70 (2004) 033802.
[18] Q. Luo, S.A. Hosseini, W. Liu, J.-F. Gravel, O.G. Kosareva, N.A. Panov, N. Aközbek, V.P. Kandidov, G. Roy, S.L. Chin, Appl. Phys. B 80 (2005) 35.
[19] J.H. Marburger, Prog. Quantum Electron. 4 (1975) 35.
[20] W. Liu, F. Theberge, J.-F. Daigle, P.T. Simard, S.M. Sarifi, Y. Kamali, H.L. Xu, S.L. Chin, Appl. Phys. B 85 (1) (2006) 55.
[21] Visionica Ltd., see <http://www.visionica.biz/index-eng.html>.
[22] Raymond M. Measures (Ed.), Laser Remote Sensing, Fundamentals and Applications, Krieger Publishing Company, Wiley, New York, 1984.
[23] Francis Théberge, Weiwei Liu, Patrick Tr. Simard, Andreas Becker, See Leang Chin, Phys. Rev. E 74 (2006) 036406.
[24] Optical-Filters.com, see <http://www.optical-filters.com/ug11.html>.